J Mater Sci: Mater Med (2011) 22:1171–1182
DOI 10.1007/s10856-011-4289-4

Development and characterization of reinforced poly(L-lactide) scaffolds for bone tissue engineering

Joo-Eon Park · Mitsugu Todo

Received: 26 October 2010 / Accepted: 10 March 2011 / Published online: 24 March 2011

Abstract Novel reinforced poly(L-lactic acid) (PLLA) scaffolds such as solid shell, porous shell, one beam and two beam reinforced scaffolds were developed to improve the mechanical properties of a standard PLLA scaffold. Experimental results clearly indicated that the compressive mechanical properties such as the strength and the modulus are effectively improved by introducing the reinforcement structures. A linear elastic model consisting of three phases, that is, the reinforcement, the porous matrix and the boundary layer was also introduced in order to predict the compressive moduli of the reinforced scaffolds. The comparative study clearly showed that the simple theoretical model can reasonably predict the moduli of the scaffolds with three phase structures. The failure mechanism of the solid shell and the porous shell reinforced scaffolds under compression were found to be buckling of the solid shell and localized buckling of the struts constructing the pores in the porous shell, respectively. For the beam reinforced scaffolds, on the contrary, the primary failure mechanism was understood to be micro-cracking within the beams and the subsequent formation of the main-crack due to the coalescence of the micro-racks. The biological study was exhibited that osteoblast-like cells, MC3T3-E1, were well adhered and proliferated on the surfaces of the scaffolds after 12 days culturing.

J.-E. Park
Interdisciplinary Graduate School of Engineering Sciences, Kyushu University, 6-1 Kasuga-koen, Kasuga 816-8580, Japan

M. Todo (✉)
Research Institute for Applied Mechanics, Kyushu University, 6-1 Kasuga-koen, Kasuga 816-8580, Japan
e-mail: todo@riam.kyushu-u.ac.jp

1 Introduction

Diseased or injured parts of bone tissue are generally treated by transplantation such as autograft and allogeneic. However, these clinical methods have disadvantages such as infection, rejection symptom and limitation in quantity [1, 2]. Over the past decade, various synthetic alternatives for bone tissue treatment have been developed using variety of materials such as metals [3–6], ceramics [7–10], polymers [11–15] and composite materials [16–21]. In general, these biomaterials have three-dimensional porous structures for cell culture and tissue ingrowth and therefore, called scaffold.

The metallic materials such as stainless steel, titanium and titanium alloys have generally been considered for the substitution of damaged bone tissues [22–26]. The main advantage of such metal implants is thought to be the excellent mechanical properties; however, there are some clinically unpleasant problems such as lack of cell adhesion, low biodegradability and difficulty in fabrication of porous structure. Furthermore, for a metal implant, a second surgery is sometimes required in order to remove the implant from the body with the related risks of toxicity due to accumulation of metal ions induced by corrosion.

Bioactivity ceramics such as hydroxyapatite (HAp), α-TCP and β-TCP consisting of calcium and phosphorous are successfully used in bone regeneration because of their components existing in natural bone and their high biocompatibility [27–33]. It is furthermore known that release of Ca^{2+} and PO_4^{3-} ions from bioactive ceramic stimulates cell proliferation and differentiation in vivo and in vitro [30–32]. However, for example, non-biodegradability of sintered HAp, relatively low strength of TCPs and the brittleness of all the bioceramics are thought to be their disadvantages [33].

On the other hand, biocompatible synthetic or natural polymers such as poly (L-lactide) (PLLA), poly (ε-caprolactone) (PCL) and collagen have been used as biomaterials for scaffold because of their biodegradability with non-biotoxic characteristics as well as moderate mechanical and physical properties [34, 35]. In recent years, bioactive ceramics such as hydroxyapatite (HAp), α-TCP and β-TCP have been used to improve the mechanical properties and the cell adherence on these polymeric scaffolds because of their compositional and structural similarities with bone and teeth [36–45].

Most of the previous researches were interested in the fabrication methods of scaffolds and described cell growth factors without structural factors such as the relationship between the mechanical properties and the porous microstructure. Some studies have been reported that the optimized porous structure of scaffold enhanced initial cell adhesion and cell migration into the scaffold [46–49]. Freed et al. [49] also insisted that well-interconnected porous structure needs to provide high surface area with sufficient space for improving cell adhesion, extracellular regeneration and minimal diffusional constrains; however, there might be a possibility for decreasing mechanical strength by the large pore size with high porosity. Therefore, a scaffold technology with controllable mechanical properties and porosity needs to be developed for seeded cells to adapt the mechanical environments, excrete a sufficient amount of extracellular matrices and accommodate a large number of cells and ensure high rate of cell growth for successful tissue regeneration [50–53].

In our previous study [54], we reported a novel core–shell structural PLLA scaffold to stimulate the mechanical properties as well as maintain high level of porosity for cell culture. The experimental results showed a successful improvement in the compressive mechanical properties and a stable porous structure under compression. In the present study, we have developed four different types of reinforcements such as solid shell, porous shell, one beam and two beams to control the mechanical and porous-structural properties by using the solid–liquid phase separation and freeze-drying methods. The compressive properties were measured and the micro-structural deformation and failure mechanisms were examined using a field-emission electron microscope (FE-SEM) in order to characterize and compare the effectiveness of the reinforcements. A simple linear elastic theory was also presented to predict the compressive modulus data. Cell culture experiment on the scaffolds was also performed with osteoblast-like MC3T3-E1 cells, and the cell adhesion morphologies were then observed using FE-SEM to compare the effect of reinforced structure on the cell adhesion behavior.

2 Materials and methods

2.1 Materials and specimen preparation

Poly(L-lactic acid) (PLLA) pellets (Lacty #5000, Shimadzu Co., Ltd) with the glass transition temperature of 69.72°C, the melting temperature of 174.9°C, the density of 1.248 g/cm^3 and the average molecular weight of 3.51 g mol^{-1} were used to fabricate scaffolds and reinforcements. Porous structures of PLLA, called mono-structural scaffolds, were fabricated by using the solid–liquid phase separation and freeze-drying methods [40, 45–49, 54]. The fabrication process of the mono scaffolds were schematically shown in Fig. 1. PLLA pellets were first dissolved in 1, 4-dioxane with a concentration of 3 wt% and then, the solutions were filled within polypropylene (PP) tubes and frozen by immersing them into liquid nitrogen from the bottom of the tubes at a constant rate of 200 mm/h. Difference of freezing behavior of the solute and the solvent induces a phase separation, resulting in the porous structure of the scaffolds. The solidified PLLA solutes were then dried under vacuum at −5°C for about 1 week to remove the solvent.

Three different kinds of reinforcement, that is, porous shell, solid shell and solid beam were adapted in this study. The fabrication processes of the reinforcements are schematically shown in Fig. 2. The porous shell reinforcements were fabricated by the same method as the mono scaffolds described in the previous section. The concentration of PLLA dioxane solution for the porous shell was chosen to be 10 wt%. A rubber tube of 8.4 mm diameter was placed in the center of a PP tube to create a shell structure as shown in Fig. 2a. The solid–liquid phase separation and subsequent freeze-drying methods were used to fabricate the porous shell structures. The mono scaffolds were then simply inserted into the central opening holes of the porous shell reinforcements to form layered structures of the porous shell reinforced scaffolds.

For the solid beam reinforcements shown in Fig. 2b, PLLA sheets of 140 × 140 × 1 mm^3 were fabricated by thermally pressing PLLA pellets using a hot press, and then beams of 2 mm width were cut out from the sheets. For the solid shell reinforcements shown in Fig. 2c, PLLA films of 250 μm thick were fabricated by hot-pressing PLLA pellets, and rectangular films of 320 mm × 140 mm × 250 μm were prepared for shell reinforcements. Those reinforcements, i.e., PLLA films or beams were then properly placed

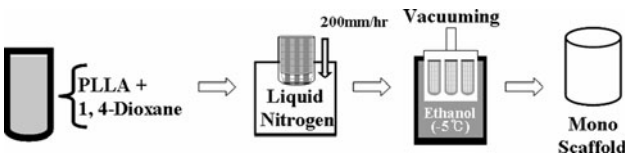

Fig. 1 Solid–liquid phase separation and freeze-drying methods

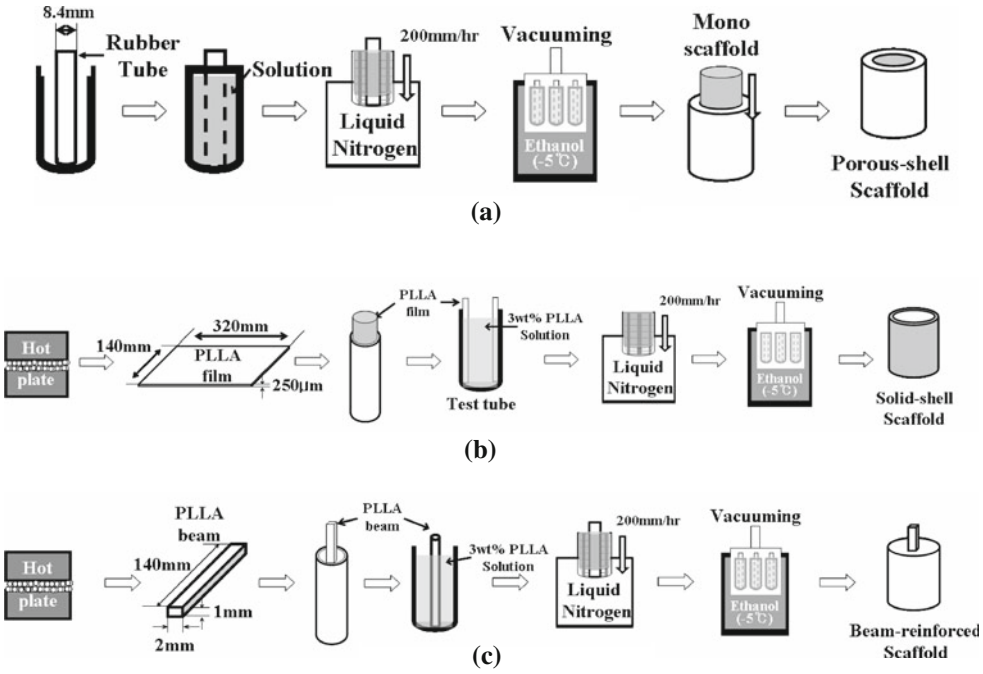

Fig. 2 Fabrication processes of reinforced scaffolds. **a** Porous-shell reinforced, **b** solid-shell reinforced, and **c** beam reinforced (one beam)

in PP tubes as shown in Fig. 2b, c. Afterward, PLLA-dioxane solutions of 3 wt% concentration were filled into the PP tubes and then frozen into liquid nitrogen as described in the previous section. After one week vacuuming process to remove the solvent, the solid shell and beam reinforced scaffolds were completed.

For the mono-structural and the beam reinforced scaffolds, cylindrical stick-type scaffolds were trimmed to be disk-type specimens with 8.5 mm diameter and 11 mm length for compression test. For the porous-shell and the solid-shell reinforced scaffolds, disk-type specimens with 11.5 mm diameter and 11 mm length were prepared for the compression test. Schematics of the cross-sections of the scaffold specimens are shown in Fig. 3.

Porosity, ϕ, of a scaffold was evaluated by the following formula:

$$\phi = \left(1 - \frac{V_{\text{PLLA}}}{V_{\text{total}}}\right) \times 100 \quad (1)$$

where V_{total} is the measured volume of the scaffold and V_{PLLA} is the volume of bulk PLLA in the scaffold. For each of the scaffold samples, the diameter and length were measured at three different positions and averaged values were then used to estimate V_{total} of the scaffold. V_{PLLA} in a scaffold was evaluated from the density, ρ, of PLLA and the weight, w_{PLLA}, of the scaffold as $V_{\text{PLLA}} = \rho w_{\text{PLLA}}$.

2.2 Compression test

The disk-type specimens described in the previous section were tested under compression by using a conventional mechanical testing machine at a displacement rate of 1 mm/min. The Four to five specimens were tested for each of the samples. Figure 4 shows a schematic of the experimental setup for the compression test. A 500 N load cell and a fixed stage were installed to the testing machine. The scaffold was positioned in the center between the crosshead and the stage. Compressive stress–strain relations were obtained from the load–displacement relations and then, the compressive modulus was calculated as the slope of the initial linear portion of the stress–strain curves. For the shell and beam reinforced scaffold specimens, the range of strain from 0.03–0.04 and 0.04–0.06 were chosen to calculate the elastic moduli, respectively. On the contrary, for the mono-structural scaffold specimens, the strain range from 0.02 to 0.03 was used to calculate the elastic modulus. The compressive strength was defined as the peak stress at a critical point where the linear elastic deformation reached the end due to the onset of irreversible deformation.

2.3 Theoretical approach

A simple linear elastic theory is introduced to predict the elastic modulus of the reinforced scaffolds. It is assumed that each of the reinforced scaffolds consists of three independent components, i.e., the reinforcement, the porous matrix and the boundary layer. The three-component model for the solid-shell scaffold is shown in Fig. 5. Under a constant displacement, δ, in the longitudinal direction, all the components are subjected by the same strain, $\varepsilon = \delta/L$, and therefore, the stresses for the components are given by:

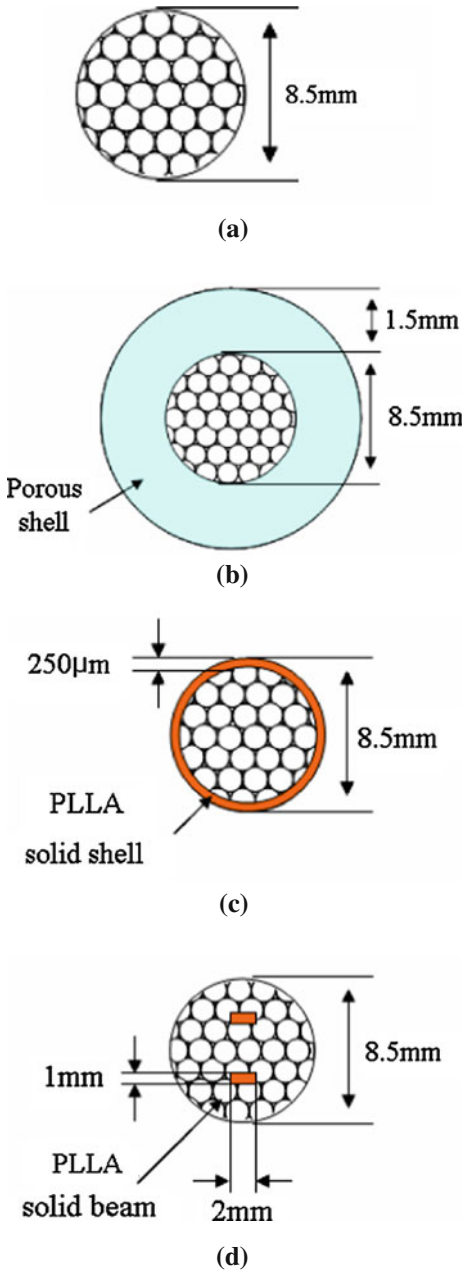

Fig. 3 Cross-sectional structures of PLLA scaffolds. **a** Mono-structural, **b** porous-shell reinforced, **c** solid-shell reinforced, and **d** beam reinforced (two beams)

$$\sigma_R = E_R\varepsilon,\ \sigma_M = E_M\varepsilon,\ \sigma_B = E_B\varepsilon \tag{2}$$

where σ is the stress, E the elastic modulus and the subscripts R, M and B denote the reinforcement, matrix and boundary layer, respectively. The equivalent elastic stress–strain relation for the reinforced scaffold is assumed to be expressed by:

$$\sigma_S = E_S\varepsilon \tag{3}$$

where E_S is the average elastic modulus of the scaffold. Since σ_S is also recognized as the average stress subjected to the scaffold, then

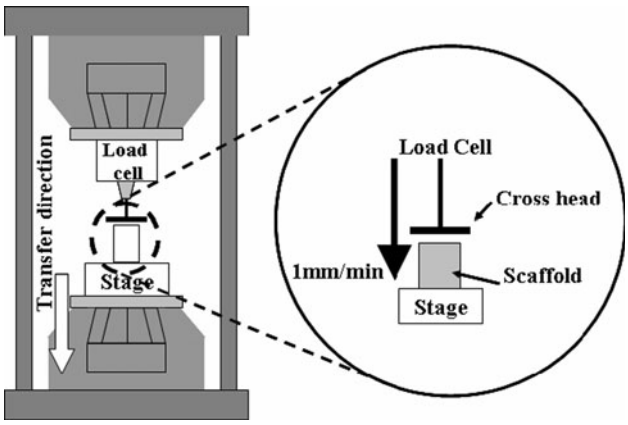

Fig. 4 Compression test set-up

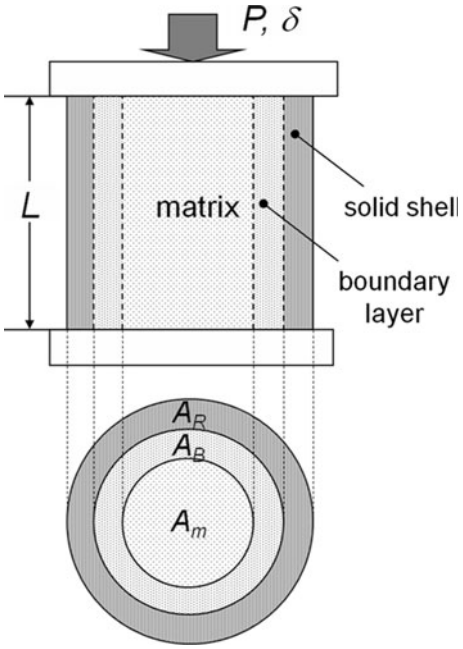

Fig. 5 Three-component model for solid shell scaffold

$$\sigma_S = \frac{P}{A_S} = \frac{1}{A_S}(\sigma_R A_R + \sigma_M A_M + \sigma_B A_B) \tag{4}$$

where P is the applied load, A the total cross-sectional area of the scaffold and A_R, A_M and A_B are the cross-sectional areas of the reinforcement, matrix and boundary layer, respectively. By substituting Eq. 2 into Eq. 4 and comparing Eqs. 4 and 3, the average modulus E_S can be expressed by:

$$E_S = \frac{1}{A_S}(E_R A_R + E_M A_M + E_B A_B) \tag{5}$$

In order to calculate E_S and compare with the experimental values, it was assumed that E_R values of the solid shell and the beam reinforcements were equivalent to the

Table 1 Properties used in the theoretical prediction of elastic moduli

	Porous-shell	Solid-shell	1 Beam	2 Beams
E_R (MPa)	41.8	322.9	322.9	322.9
E_M (MPa)	5.52	5.52	5.52	5.52
E_B (MPa)	111	111	111	111
A_S (mm^2)	102.1	57.1	45.4	47.5
A_M (mm^2)	55.4	51.6	37.9	35.6
A_R (mm^2)	46.7	3.47	1.44	2.88
A_B (mm^2)	–	1.97	6.0	9.0

elastic modulus of bulk PLLA that was evaluated by compression tests of bulk PLLA specimens. E_R of the porous shell was chosen as the modulus of the mono-structural scaffold made from 10 wt% PLLA solution. For all the reinforced scaffolds, E_M was assumed to be equivalent to the modulus of the mono-structural scaffold made from 3 wt% PLLA solution. E_B was assumed to be equal to the modulus of the mono-structural scaffold made from 30 wt% PLLA solution on the basis of structural analysis of the porous structure of the boundary layer using FE-SEM micrographs. The cross-sectional areas were directly measured from FE-SEM micrographs. The data used in this theoretical analysis are shown in Table 1.

2.4 Microstructural characterization

The porous microstructures of the scaffolds were characterized using a field emission scanning electron microscope (FE-SEM) (S-4100, Hitachi, Japan). FE-SEM was also utilized to characterize the deformation mechanism at the critical point. Undeformed and deformed samples of the scaffolds were cut into about 5 mm pieces by flesh razor blades after frozen in liquid nitrogen for several minutes and placed on aluminum disks using carbon tapes, and the entire surfaces were coated with Pt–Pd using an Ion sputter coater (E-1030, Hitachi, Japan).

2.5 Cultivation of MC3T3-E1 cells

Osteoblast-like cells, MC3T3-E1, were cultured with ascorbic-free α-MEM supplements with 1% penicillin–streptomycin and 10% FBS in a 60 mm^2 cell culture dish, and the culture medium was changed every 2 days. The culture dishes were placed in a humidified incubator at 37°C with 95% air/5% CO_2 (v/v) during cell culturing. The cells were counted using a hemacytometer every subculture day. The cultured cells were suspended at the concentration of 5×10^4 cells/μl in fresh medium to seed on the scaffolds. The cell suspensions of high concentration of 10 μl were seeded onto the surfaces of pre-wetted scaffolds. The scaffolds were submerged in ethanol for 1 h and then soaked in PBS three times (30 min each). After sterilizing, the scaffolds were then washed in prepared culture medium twice (2 h each). The cell-seeded scaffolds were then placed in the humidified incubator and the medium was changed every 2 days. Adhesion behavior of MC3T3-E1 cells on the surfaces of the scaffolds were observed after 12 days of cell seeding.

3 Results and discussion

3.1 Porosity and microstructure

Porosity is thought to be one of the most important key factors in designing scaffold for cell cultivation. Li et al. [55] reported that the suitable porosity for improving cell adhesion was more than 80%. Porosity values of the scaffolds estimated by Eq. 1 are shown in Table 2. The averaged porosities of the reinforced scaffolds were lower than that of the mono-structural scaffold, however, still higher than 80%. Such reduction of the averaged porosity is obviously related to the existence of solid or dense reinforcements in the scaffolds. Although the averaged porosity decreases due to reinforcements, the fundamental porosities of the porous matrices were almost the same as the mono scaffold as shown in Table 2 in which the averaged porosities and the porosities of the porous shell and the matrices are presented.

FE-SEM micrographs of the microstructures of the scaffolds are shown in Fig. 6. Homogeneous distributions of pores are observed in all the scaffolds. In the porous-shell scaffold (Fig. 6b), there exists a small gap between the porous-outer shell and the core region because a mono scaffold was simply inserted into the porous shell reinforcement. Figure 6c, d clearly show that the solid shell and the beam reinforcement were firmly connected to the porous matrix regions. It is noted that a porous boundary region existed between the reinforcement and the porous-matrix and had less porosity and smaller pore sizes than the porous matrix region. It is thought that the solid reinforcements were slightly dissolved into the PLLA solution

Table 2 Porosity values of PLLA scaffolds

Specimen	Averaged porosity (%)	Reinforcement (%)	Porous matrix (%)
Mono-structural	94.84	–	–
Porous shell	88.11	80.34	94.84
Solid shell	82.91	–	93.74
1 Beam	88.85	–	93.64
2 Beams	83.6	–	92.39

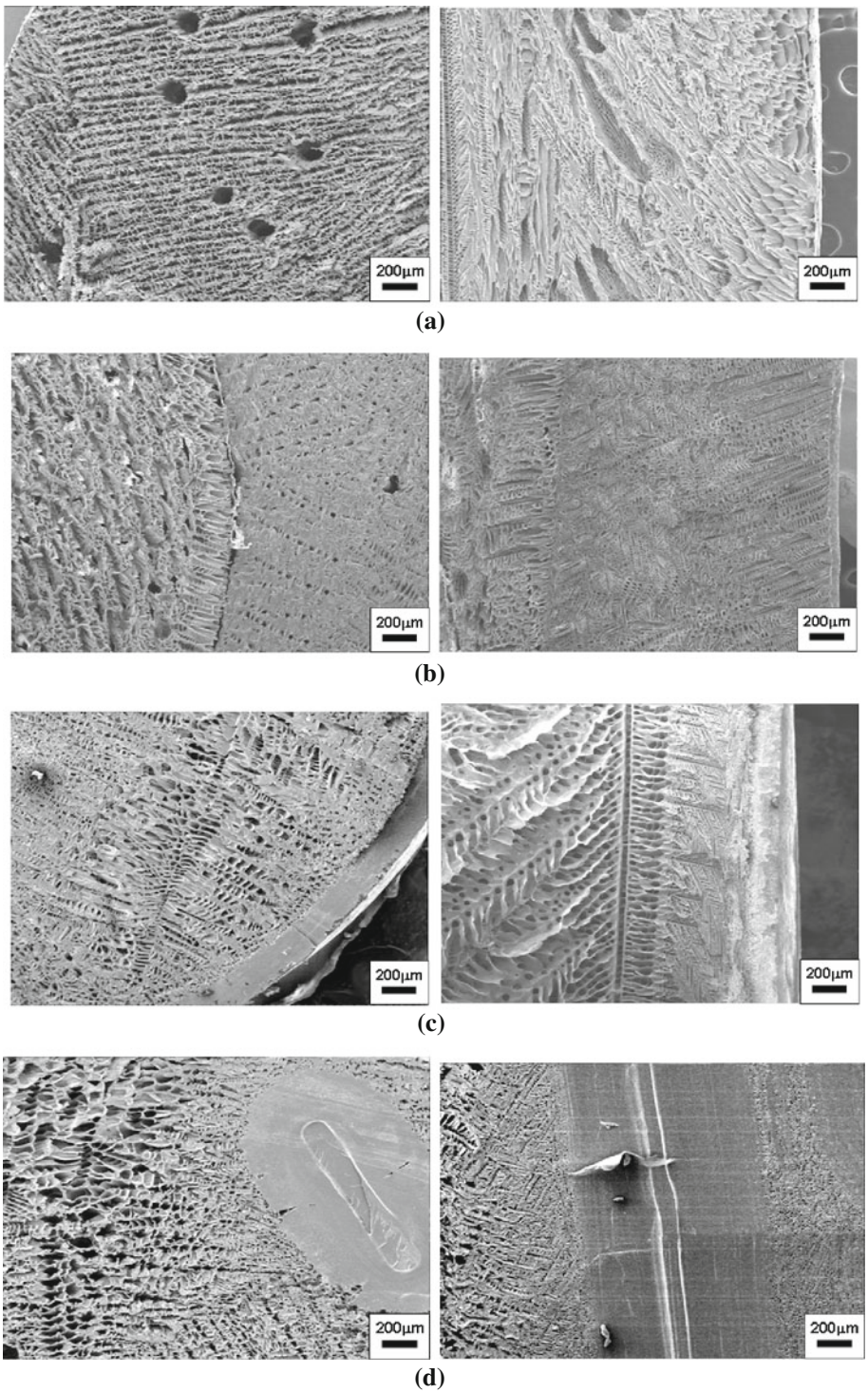

Fig. 6 FE-SEM micrographs of microstructures of PLLA scaffolds. The *left*- and the *right*-hand sides are the cross-sections and the longitudinal sections, respectively. **a** Mono-structural, **b** porous-shell reinforced, **c** solid-shell reinforced, and **d** beam reinforced (one beam)

during fabrication process and then, the boundary regions were created. This phenomenon is also explaining why the porosities of porous matrices in the reinforced scaffolds slightly decreased compared to that in the mono-structural scaffold as shown in Table 2. In case of the solid shell and the beam reinforced scaffolds, the densities of the porous matrices slightly increased due to the dissolution of the reinforcements into the matrices, resulting in slight decrease of porosities of the matrices.

3.2 Compressive mechanical properties

Typical stress–strain curves obtained from the compression tests and schematic drawings of the stress–strain relations

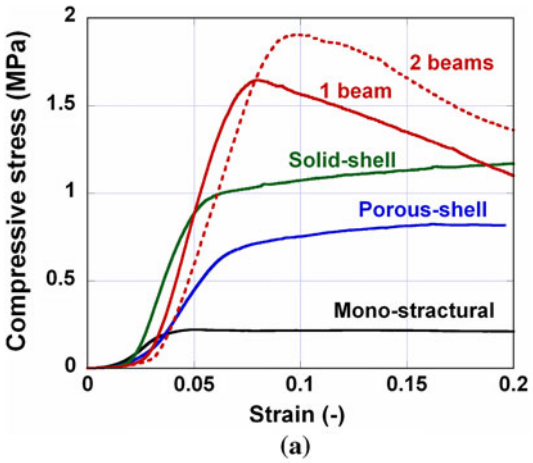

Fig. 7 Stress-strain relations in PLLA scaffolds. **a** Typical stress–strain curves and **b** schematic of stress–strain relations

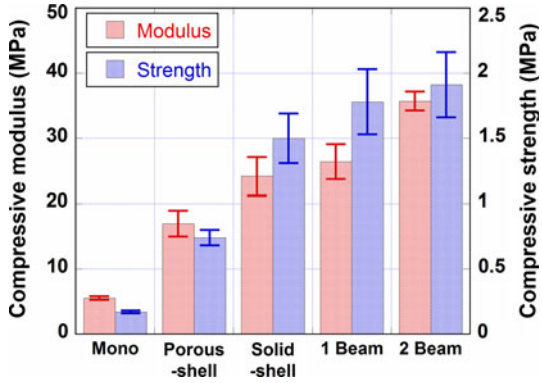

Fig. 8 Compressive mechanical properties of PLLA scaffolds

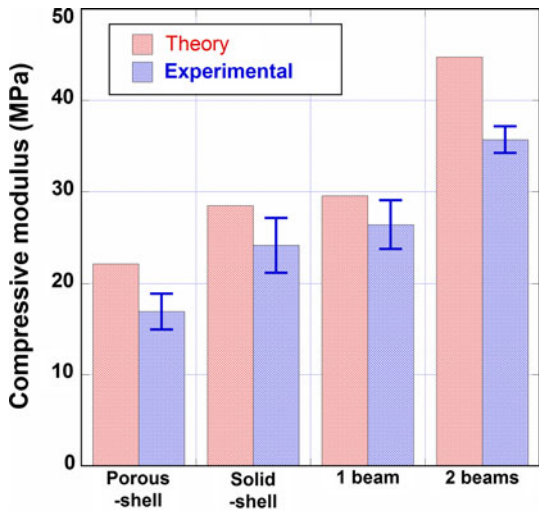

Fig. 9 Elastic modulus of theoretical and experimental results of PLLA scaffolds

are shown in Figure 7a, b. The stress–strain relations are basically divided into four regions based on their deformation behaviors as shown in Fig. 7b. The region 1 is characterized by the gentle slope mainly due to the misalignment between the specimen upper surface and the loading device. The region 2 is recognized as the initial linear portion corresponding to the global linear elastic deformation of the scaffolds. The compressive moduli were evaluated as the slopes of these regions. The region 3 contains the critical point at which the global elastic deformation was ended due to local irreversible deformations such as microbuckling of the struts constructing pore structures or delamination between the reinforcements and the porous matrices. In the region 4, the stresses slightly increased in the shell reinforced scaffolds, gradually decreased in the beam reinforced scaffolds or was almost constant in the mono-structural scaffold. These different behaviors were caused by the different failure modes discussed in the Sect. 3.3. It is clearly seen from Fig. 7b that the slope of the region 2, corresponding to the elastic modulus, and the stress level at the critical point increased due to the introduction of the reinforcements, suggesting the improvement of the modulus and the strength. It is noted that characterization of the relationship between the deformation mechanism and the stress–strain relation in the whole range of strain from 0 to 1 is also important in order to understand the mechanical response of scaffolds under compression. Such characterization for PLLA scaffolds has been discussed in our previous paper [12].

The compressive elastic modulus and the strength are shown in Fig. 8. It is clearly seen that both the modulus and the strength were effectively improved by introducing the reinforcements. The compressive properties of the beam reinforced scaffolds were higher than those of the shell reinforced scaffolds. The theoretical values of the modulus obtained from Eq. 5 are compared with the experimental in Fig. 9. The theory well predicts the tendency of the reinforcement effects, however, tends to result in overestimation. The deformation of the reinforced porous structures may differ from the simple linear elastic solid model constructed in this study.

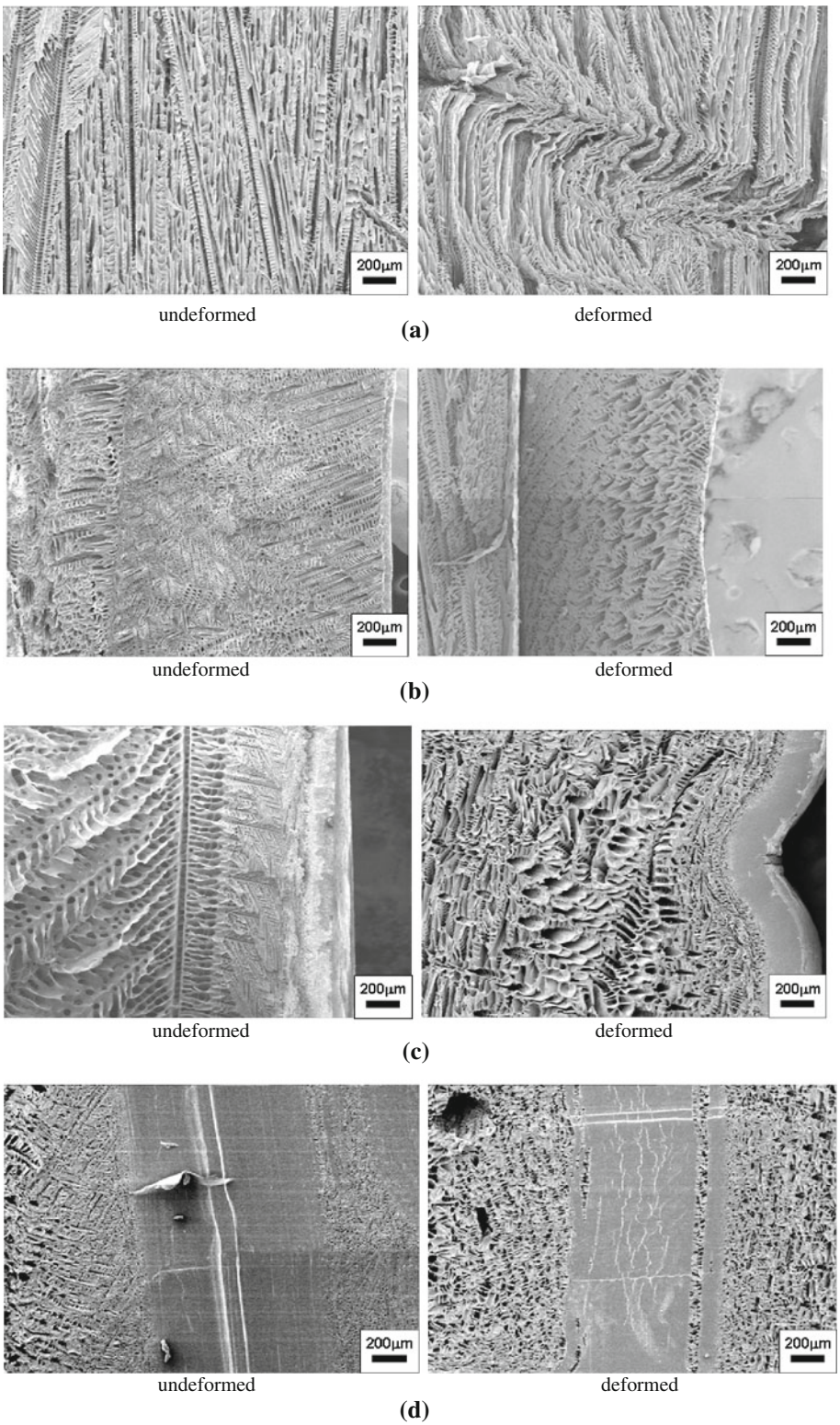

Fig. 10 FE-SEM micrographs of deformed PLLA scaffolds at the critical point. **a** Mono-structural, **b** porous-shell reinforced, **c** solid-shell reinforced, and **d** beam reinforced (one beam)

3.3 Deformation and failure behaviors at critical point

FE-SEM micrographs of undeformed and deformed scaffolds are shown in Fig. 10. FE-SEM micrographs of the deformed reinforced scaffolds at a higher magnification are also shown in Fig. 11. The deformed samples were obtained at the critical points. The failure mechanism of the mono-structural scaffold at the critical point is characterized by a series of localized buckling of the struts. In the porous-shell reinforced scaffold, the most of compressive

load is supported by the porous-shell having a higher stiffness than the porous matrix and therefore, the critical point was initiated by the irreversible deformation of the porous-shell. The primary mechanism of such deformation is localized buckling of the struts and also shown in Fig. 11a. It is seen that the struts were totally collapsed under compression. In the solid-shell reinforced scaffold, the main failure mechanism is understood to be buckling deformation of the solid outer shell as shown in Figs. 10c and 11b. In the beam reinforced scaffold, the failure mechanism is characterized by micro-cracking and subsequent larger-scale cracking within the beam reinforcement as shown in Figs. 10d, 11c. The micro-cracking is thought to be generated by the tensile strain induced as the Poisson's effect in the direction perpendicular to the compressive direction. Those micro-cracks are connected each other under further strained condition and finally the main cracks are created.

It is thus understood that in all the reinforced scaffolds, compressive load is mainly supported by the reinforcements and therefore, the porous matrix in which cells are mainly cultured keeps its original porous structure until the reinforcements are severely deformed, while the mono-structural scaffold is easily deformed and collapsed in the earlier stage of compression loading.

3.4 Proliferation of MC3T3-E1 cells

Adhered MC3T3-E1 cells on the surfaces of the scaffolds are shown in Fig. 12. It is clearly shown that MC3T3-E1 cells were well adhered on the various surfaces of the scaffolds after 12 days culturing. In the mono-structural scaffold, however, the cells were attached only on the limited surface area. In contrast, the cells were spread over the wider surface areas in the reinforced scaffolds. Liu et al. [56] demonstrated that the surface morphology of a scaffold is an important factor for adhesion and growth of cells. It is also confirmed that MC3T3-E1 cells showed better adhesion and proliferation behavior on the discontinuous surfaces of the reinforced scaffolds with the small-large pores (porous-shell), porous-dense-porous (beam-reinforced) and dense-porous (solid-shell) surfaces than the homogeneous porous surface on the mono-structural scaffold. It is thus considered that such discontinuity of surface morphology in the reinforced scaffolds stimulates the proliferation of cells, and therefore, the number of cells effectively increases.

It is concluded on the basis of those experimental results that the newly developed reinforced scaffolds have a non-toxic character and higher mechanical properties and therefore, may have better applicability than the mono-structural scaffold.

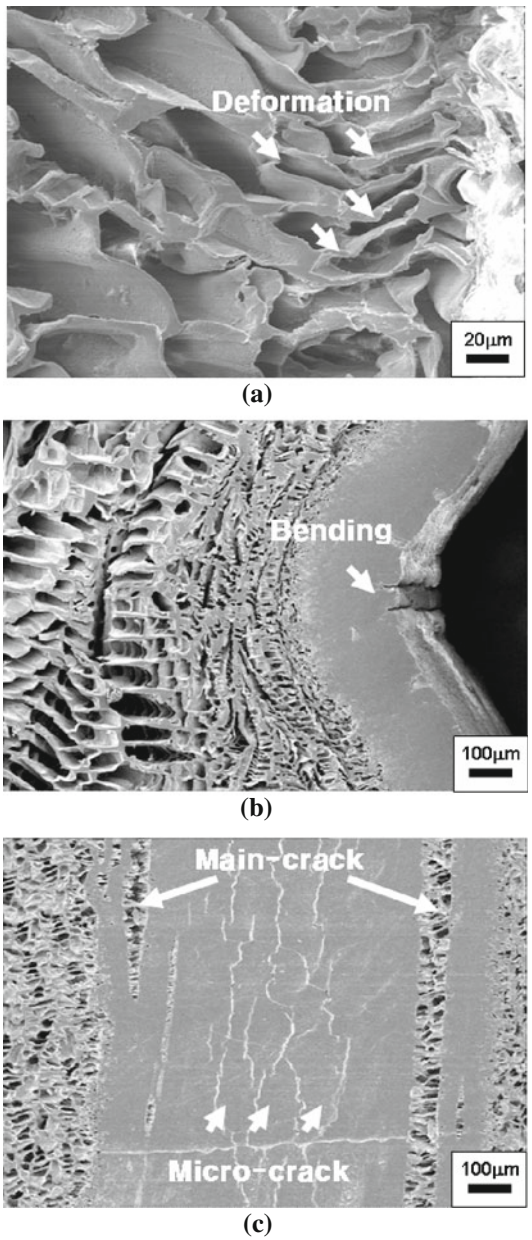

Fig. 11 Deformation mechanisms of reinforced scaffolds. **a** Porous-shell reinforced, **b** solid-shell reinforced, and **c** beam reinforced (one beam)

4 Conclusions

Novel reinforced porous poly(L-lactic acid) scaffolds were developed introducing four different kinds of reinforcements, that is, solid shell, porous shell, one beam and two beams by the solid–liquid phase separation and the freeze-drying methods. The conclusions were obtained as follows:

(1) Compressive mechanical properties such as the elastic modulus and the strength were effectively improved by the reinforced structures. The beam

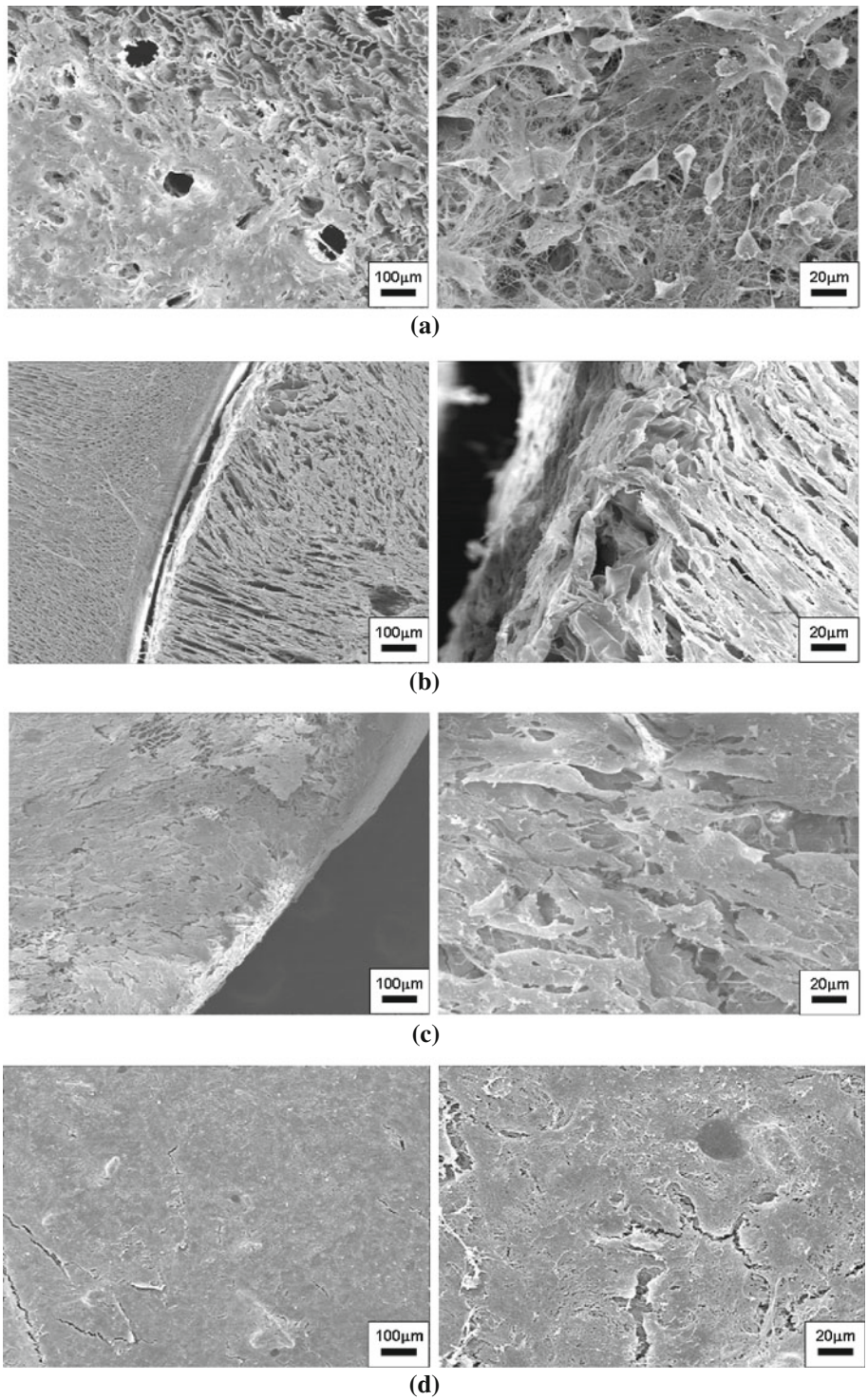

Fig. 12 Adhesion behaviors of MC3T3-E1 cells on PLLA scaffolds. **a** Mono-structural, **b** porous-shell reinforced, **c** solid-shell reinforced, and **d** beam reinforced (one beam)

reinforced scaffolds exhibited higher mechanical properties than the core–shell scaffolds.

(2) A simple theoretical approach on the basis of the linear elastic mechanics was presented in order to predict the compressive elastic moduli of the reinforced scaffolds. A three-phase model was introduced and the analytical results well coincided with the experimental results.

(3) In the solid shell reinforced scaffold, the primary failure mechanism at the critical point was characterized by the buckling of the solid shell under compressive loading. In the porous shell reinforced

scaffold, the porous shell was mainly deformed at the critical point, and the main mechanism of failure was the localized buckling of the struts constructing the pores in the porous shell. For the beam reinforced scaffolds, the primary failure mechanism was found to be the micro-cracking within the beams and the subsequent formation of the main-crack due to the coalescence of the micro-racks.

(4) MC3T3-E1 cells were well adhered and proliferated on the surfaces of the scaffolds. The cells were more widely adhered on the reinforced scaffolds than the mono-structural scaffold.

References

1. De Bore HH. The history of bone grafts. Clin Orthop Relat Res. 1988;226:292–8.
2. Vacanti CA, Kim W, Upton J, et al. Tissue-engineered growth of bone and cartilage. Transplant Proc. 1993;25:1019–21.
3. Dolde JVD, Farber E, Spauwen PHM, Jansen JA. Bone tissue reconstruction using titanium fiber mesh combined with rat bone marrow stromal cells. Biomaterials. 2003;24:1745–50.
4. Nienhuijs MEL, Walboomers XF, Merkx MAW, et al. Bone-like tissue formation using an equine COLLOSS® E-filled titanium scaffolding material. Biomaterials. 2006;27:3109–14.
5. Fujibayashi S, Neo M, Kim HM, et al. Osteoinduction of porous bioactive titanium metal. Biomaterials. 2004;25:443–50.
6. Li JP, Wijn JRD, Blitterswijk CAV, Groot KD. Porous Ti6Al4V scaffold directly fabricating by rapid prototyping: preparation and in vitro experiment. Biomaterials. 2006;27:1223–35.
7. Dellinger JG, Eurell JAC, Jamison RD. Bone response to 3D periodic hydroxyapatite scaffolds with and without tailored microporosity to deliver bone morphogenetic protein 2. J Biomed Mater Res. 2005;76A:366–76.
8. Deville S, Saiz E, Tomsia AP. Freeze casting of hydroxyapatite scaffolds for bone tissue engineering. Biomaterials. 2006;27:5480–9.
9. Yuan H, Bruijn JD, Li Y, et al. Bone formation induced by calcium phosphate ceramics in soft tissue of dogs: a comparative study between porous α-TCP and β-TCP. J Mater Sci Mater Med. 2001;12:7–13.
10. Wiltfang J, Merten HA, Schlegel KA, et al. Degradation characteristics of α and β tri-calcium-phosphate (TCP) in minipigs. J Biomed Mater Res. 2002;63:115–21.
11. Reverchon E, Cardea S, Rapuano C. A new supercritical fluid-based process to produce scaffolds for tissue replacement. J Supercrit Fluids. 2008;45:365–73.
12. Todo M, Kuraoka H, Kim JW, et al. Deformation behavior and mechanism of porous PLLA under compression. J Mater Sci. 2008;43:5644–6.
13. Lin ASP, Barrows TH, Cartmell SH, Guldberg RE. Microarchitectural and mechanical characterization of oriented porous polymer scaffolds. Biomaterials. 2003;24:481–9.
14. MA L, Gao C, Mao Z, et al. Collagen/chitosan porous scaffolds with improved biostability for skin tissue engineering. Biomaterials. 2003;24:4833–41.
15. Seda Tığlı R, Karakeçili A, Gümüşderelioğlu M. In vitro characterization of chitosan scaffolds: influence of composition and deacetylation degree. J Mater Sci Mater Med. 2007;18:1665–74.
16. Ghosh S, Viana JC, Reis RL, Mano JF. Bi-layered constructs based on poly(L-lactic acid) and starch for tissue engineering of osteochondral defects. Mater Sci Eng C. 2008;28:80–6.
17. Wei G, Ma PX. Structure and properties of nano-hydroxyapatite/polymer composite scaffolds for bone tissue engineering. Biomaterials. 2004;25:4749–57.
18. Miao X, Tan DM, Li J, Xiao Y, Crawford R. Mechanical and biological properties of hydroxyapatite/tricalcium phosphate scaffolds coated with poly(lactic-co-glycolic acid). Acta Biomater. 2008;4:638–45.
19. Yang XB, Webb D, Blaker J, et al. Evaluation of human bone marrow stromal cell growth on biodegradable polymer/bioglass composites. Biochem Biophys Res Commun. 2006;342:1098–107.
20. Yamamoto M, Takahashi Y, Hokugo A, Tabata Y. Enhanced osteoinduction by controlled release of bone morphogenetic protein-2 from biodegradable sponge composed of gelatin and b-tricalcium phosphate. Biomaterials. 2005;26:4856–65.
21. Tanaka T, Eguchi S, Satoh H, et al. Microporous foams of polymer blends of poly(L-lactic acid) and poly(ε-caprolactone). Desalination. 2008;234:175–83.
22. Oron A, Agar G, Oron U, Stein A. Correlation between rate of bony ingrowth to stainless steel, pure titanium, and titanium alloy implants in vivo and formation of hydroxyapetite on their surfaces in vitro. J Biomed Mater Res. 2008;91A:1006–9.
23. Wall EJ, Jain V, Vora V, Mehlman CT, Crawford AH. Complications of titanium and stainless steel elastic nail fixation of pediatric femoral fractures. J Bone Joint Surg Am. 2008;90:1305–13.
24. Niinomi M. Mechanical biocompatibilities of titanium alloys for biomedical applications. J Mecha Behav Biomed Mater. 2008;1:30–42.
25. Zhang E, Xu L, Yu G, et al. In vivo evaluation of biodegradable magnesium alloy bone implant in the first 6 months implantation. J Biomed Mater Res. 2009;90A:882–93.
26. Chen J, Birch MA, Bull SJ. Nanomechanical characterization of tissue engineered bone grown on titanium alloy in vitro. J Mater Sci Mater Med. 2010;21:277–82.
27. Tadic D, Beckmann F, Schwarz K, Epple M. A novel method to produce hydroxyapatite objects with interconnectingporosity that avoids sintering. Biomaterials. 2004;25:3335–40.
28. Matsumura K, Hyon SH, Nakajima N, et al. Surface modification of poly(ethylene-co-vinyl alcohol): hydroxyapatite immobilization and control of periodontal ligament cells differentiation. Biomaterials. 2004;25:4817–24.
29. Webster TJ, Ergun C, Doremus RH, et al. Enhanced functions of osteoblasts on nanophase ceramics. Biomaterials. 2000;21:1803–10.
30. Chen QZ, Efthymiou A, Salih V, Boccaccini AR. Bioglass®-derived glass–ceramic scaffolds: study of cell proliferation and scaffold degradation in vitro. J Biomed Mater Res. 2007;84A:1049–60.
31. Bignon A, Chouteau J, Chevalier J, et al. Effect of micro- and macroporosity of bone substitutes on their mechanical properties and cellular response. J Mater Sci Mater Med. 2003;14:1089–97.
32. Peroglio M, Gremillard L, Chevalier J, et al. Toughening of bioceramics scaffolds by polymer coating. J Eur Ceram Soc. 2007;27:2679–85.
33. Rezwana K, Chena QZ, Blakera JJ, Boccaccini AR. Biodegradable and bioactive porous polymer/inorganic composite scaffolds for bone tissue engineering. Biomaterials. 2006;27:3413–31.
34. Todo M, Park JE, Kuraoka H, et al. Compressive deformation behavior of porous PLLA/PCL polymer blend. J Mater Sci. 2009;44:4191–4.
35. Kim SS, Park MS, Jeon OJ, et al. Poly(lactide-co-glycolide) hydroxyapatite composite scaffolds for bone tissue engineering. Biomaterals. 2006;27:1399–409.

36. Simon JL, Rekow ED, Thompson VP, et al. MicroCT analysis of hydroxyapatite bone repair scaffolds created via three-dimensional printing for evaluating the effects of scaffold architecture on bone ingrowth. J Biomed Mater Res. 2007;85A:371–7.
37. George J, Kuboki Y, Miyata T. Differentiation of mesenchymal stem cells into osteoblasts on honeycomb collagen scaffolds. Biotech Bioeng. 2006;95:404–11.
38. Yunos DM, Bretcanu O, Boccaccini AR. Polymer-bioceramic composites for tissue engineering scaffolds. J Mater Sci. 2008;43:4433–42.
39. Kang Y, Yin G, Yuan Q, et al. Preparation of poly(L-lactic acid)/β-tricalcium phosphate scaffold for bone tissue engineering without organic solvent. Mater Lett. 2008;62:2029–32.
40. O'Brien FJ, Harley BA, Yannas IV, Gibson LJ. The effect of pore size on cell adhesion in collagen-GAG scaffolds. Biomaterials. 2005;26:433–41.
41. Georgiou G, Mathieu L, Pioletti DP, et al. Polylactic acid–phosphate glass composite foams as scaffolds for bone tissue engineering. J Biomed Mater Res. 2007;80B:322–31.
42. Tsivintzelis I, Pavlidou E, Panayiotou C. Porous scaffolds prepared by phase inversion using supercritical CO_2 as antisolvent: I. Poly(L-lactic acid). J Supercrit Fluids. 2007;40:317–22.
43. Maquet V, Boccaccini AR, Pravata L, et al. Preparation, characterization, and in vitro degradation of bioresorbable and bioactive composites based on Bioglass®-filled polylactide foams. J Biomed Mater Res. 2003;66A:335–46.
44. Ang TH, Sultana FSA, Hutmacher DW, et al. Fabrication of 3D chitosan–hydroxyapatite scaffolds using a robotic dispensing system. Mater Sci Eng C. 2002;20:35–42.
45. Teng X, Ren J, Gu S. Preparation and characterization of porous PDLLA/HA composite foams by supercritical carbon dioxide technology. J Biomed Mater Res. 2006;81B:185–93.
46. Oh SH, Park IK, Kim JM, Lee JH. In vitro and in vivo characteristics of PCL scaffolds with pore size gradient fabricated by a centrifugation method. Biomaterials. 2007;28:1664–71.
47. Murphy CM, Haugh MG, O'Brien FJ. The effect of mean pore size on cell attachment, proliferation and migration in collagen–glycosaminoglycan scaffolds for bone tissue engineering. Biomaterials. 2010;31:461–6.
48. Karageorgiou V, Kaplan D. Porosity of 3D biomaterial scaffolds and osteogenesis. Biomaterials. 2005;26:5474–91.
49. He X, Lu H, Kawazoe N, Tateishi T, Chen G. A novel cylinder-type poly(L-lactic acid)–collagen hybrid sponge for cartilage tissue engineering. Tissue Eng C Methods. 2010;16:329–38.
50. Young CS, Terada S, Vacanti JP, et al. Tissue engineering of complex tooth structures on biodegradable polymer scaffolds. J Dent Res. 2002;81:695–700.
51. Tu C, Cai Q, Yang J, et al. The fabrication and characterization of poly(lactic acid) scaffolds for tissue engineering by improved solid-liquid phase separation. Polym Adv Technol. 2003;14:565–73.
52. Hu FJ, Park TG, Lee DS. A facile preparation of highly interconnected macroporous poly(D, L-lactic acid-co-glycolic acid) (PLGA) scaffolds by liquid–liquid phase separation of a PLGA–dioxane–water ternary system. Polymer. 2003;44:1911–20.
53. Woo KM, Seo JH, Zhang R, Ma PX. Suppression of apoptosis by enhanced protein adsorption on polymer/hydroxyapatite composite scaffolds. Biomaterials. 2007;28:2622–30.
54. Park JE, Todo M. Development of layered porous poly(L-lactide) for bone regeneration. J Mater Sci. 2010;45:3966–8.
55. Li X, Feng Q, Cui F. In vitro degradation of porous nano-hydroxyapatite collagen PLLA scaffold reinforced by chitin fibres. Mater Sci Eng C. 2006;26:716–20.
56. Liu HC, Lee IC, Wang JH, et al. Preparation of PLLA membraines with different morphologies for culture of MG-63 cells. Biomaterials. 2003;25:4047–56.